35th Annual International Conference of the IEEE EMBS
Osaka, Japan, 3 - 7 July, 2013

Automatic Removal of Manually Induced Artefacts in Ultrasound Images of Thyroid Gland

Nikhil S. Narayan[1], Pina Marziliano[1] and Christopher G.L. Hobbs, MD[2]

Abstract— **Manually induced artefacts, like caliper marks and anatomical labels, render an ultrasound (US) image incapable of being subjected to further processes of Computer Aided Diagnosis (CAD). In this paper, we propose a technique to remove these artefacts and restore the image as accurately as possible. The technique finds application as a pre-processing step when developing unsupervised segmentation algorithms for US images that deal with automatic estimation of the number of segments and clustering. The novelty of the algorithm lies in the image processing pipeline chosen to automatically identify the artefacts and is developed based on the histogram properties of the artefacts. The algorithm was able to successfully restore the images to a high quality when it was executed on a dataset of 18 US images of the thyroid gland on which the artefacts were induced manually by a doctor. Further experiments on an additional dataset of 10 unmarked US images of the thyroid gland on which the artefacts were simulated using Matlab showed that the restored images were again of high quality with a PSNR $>$ 38dB and free of any manually induced artefacts.**

I. INTRODUCTION

The diagnosis and treatment of thyroid diseases is based on the size of the finding in the Ultrasound (US) Image. The usual procedure is to manually mark, using digital calipers, the regions of thyroid/nodule having maximum dimensions and measure the maximum sizes on the US image. Further, to indicate the region being imaged, a label corresponding to the anatomical structure is applied on the image. The image along with the marks are then saved in a storage device for future use. In this paper, we address the use of these marked US images in the context of developing Computer Aided Diagnosis (CAD) algorithms applied to the Thyroid gland. In the rest of the paper, the caliper marks and the labels will be referred to as the artefacts and the image region within which these occur will be referred to as the Region of Interest (ROI).

The importance of choosing the right type of data for CAD algorithms has been a topic of much interest since the early 90's when CAD started to gain momentum with the advent of new technologies in medical imaging. Nishikawa et al., [9] in their paper on case selection for CAD, noted that the sensitivity of the CAD algorithms dropped to as low as 26% with the wrong type of dataset used for training and testing.

In our recent work on developing a fully unsupervised algorithm to segment an US image of the thyroid gland, the presence of manually induced artefacts significantly affected the results of the algorithm [8]. We had developed an algorithm that automatically estimates the number of clusters in the input US image based on tissue echogenicity, which then performs segmentation of the US image by classifying the pixels into the estimated clusters. The presence of manually induced artefacts resulted in the number of estimated clusters to be one higher than the actual number of clusters, that in turn resulted in false positive classification of the pixels as the algorithm builds a classifier based on the properties of the pixels in the cluster. This is illustrated in Figure 1, where the pixels representing the soft tissue bordering the muscles and some pixels of the soft tissue bordering the thyroid gland have been misclassified as that belonging to the artefact instead of soft tissue. Speaking in terms of Ultrasound Nomenclature [3], if the segmentation algorithm were to detect only the hyperechoic regions in the US image, then, due to the presence of manually induced artefacts, the algorithm picks up all the pixels associated with the artefacts instead of the soft tissue pixels as the artefacts tend to have a brightness value that mimics the brightness of the hyperechoic tissue pixels. Although not reported, this can be a major issue in existing algorithms that use automatic cluster estimation for US image segmentation like in [1].

With the growing interest in automatic cluster estimation and cluster validity [4]–[6], [11], [12], and with the focus of research in Medical Imaging shifting towards developing applications for e-Health and portable hand held devices [10], it is only a matter of time before all algorithms tend to follow an unsupervised model without being restricted for use just in hospitals and point of care establishments. Under such circumstances, the algorithms must be robust, capable of handling any type of data and give reliable results, which is not possible if the algorithms are developed purely based on carefully selected datasets like the ones in the databases of [2] and [7], where any image dataset having image artefacts is not considered and, if present, are discarded from the database.

Acquiring any dataset is a time consuming and expensive process, discarding a dataset would not only be a costly affair but also tend to make the algorithms developed more sensitive to artefacts. This brings the need to develop a robust pre-processing algorithm that can be used to detect and remove the artefacts, thereby enabling the data to be used in other CAD applications. It should be noted here that the purpose of the pre-processing algorithm is to aid in the development of CAD algorithms and the pre-processed images cannot directly be used for diagnosis purposes if the

*The authors would like to acknowledge the Ph.D. grant from the Institute for Media Innovation, Nanyang Technological University, Singapore.

[1]N.S. Narayan and P. Marziliano are with the Department of Electrical and Electronic Engineering, Nanyang Technological University, Singapore, nikhilna001@e.ntu.edu.sg and epina@ntu.edu.sg.

[2]C.G.L. Hobbs is with the Department of Otorhinolaryngology, Tan Tock Seng Hospital, Singapore, christopher_hobbs@ttsh.com.sg.

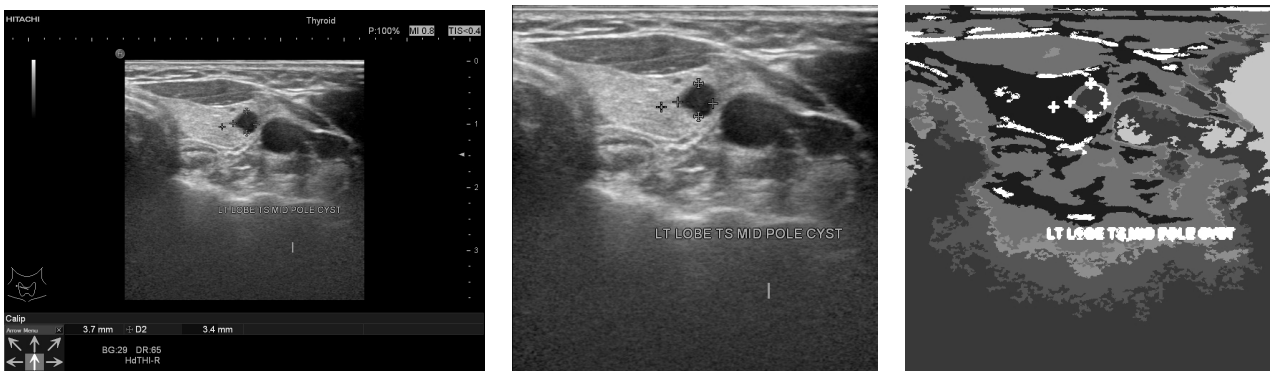

(a) Input US image (b) ROI (c) Segmented Image

Fig. 1. Automatic cluster estimation and unsupervised segmentation of the ultrasound image of a thyroid gland showing false positive classification of pixels due to manually induced artefacts.

artefacts are at such regions that affect further diagnosis.

With this in mind, we propose in this paper a technique to automatically detect the artefacts; remove them and restore the artefact removed image as accurately as possible. We claim novelty on the image processing pipeline proposed to automatically detect the artefacts using the limited amount of histogram based information available on the artefacts.

II. Our Approach

The flow of the algorithm is shown in Fig.2.

A. Stage 1: Artefact Removal

The first stage in the algorithm is to determine the properties of the artefacts introduced in the ROI and to suppress the artefacts. The property of the artefact that we are interested in is the intensity level as it remains the same for all the artefacts irrespective of the shape for a given imaging device.

1) Extracting the ROI: Since we are dealing with the artefacts present within the ROI, the first task is to automatically identify the ROI in the $m \times n$ input US image denoted by $f(x, y) \in [0, 255]$. It can be seen from Fig. 3 that the ROI is the largest component in the whole image. So the binary image of $f(x, y)$ is obtained by Eq.(1)

$$b_0(x, y) = \begin{cases} 1 & \text{if } f(x, y) > 0 \\ 0 & \text{otherwise} \end{cases} . \tag{1}$$

Applying 2D connected components algorithm on the binary image $b_0(x, y)$ results in a labelled image $s(x, y)$ with K components, given by

$$s(x, y) = l; \quad l \in [1, K]. \tag{2}$$

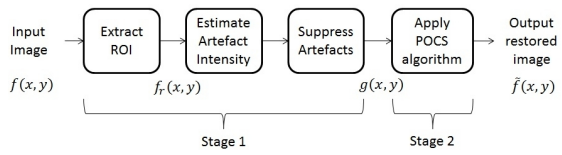

Fig. 2. Flow diagram of the algorithm

Letting $l_{\max}$ to be the label of the component in $s(x, y)$ with the maximum number of pixels in it, define a binary mask $r(x, y)$ such that

$$r(x, y) = \begin{cases} 1 & \text{if } s(x, y) = l_{\max} \\ 0 & \text{otherwise} \end{cases} . \tag{3}$$

The image containing just the ROI, $f_r(x, y)$ and its complement $\bar{f}_r(x, y)$ are given by

$$f_r(x, y) = f(x, y) \cdot r(x, y) \tag{4}$$

$$\bar{f}_r(x, y) = f(x, y) - f_r(x, y). \tag{5}$$

2) Estimating artefact intensity: Once $\bar{f}_r(x, y)$ is obtained, its histogram is plotted. Since $\bar{f}_r(x, y)$ is independent of the ROI, it is very clear that the filled bins of the histogram directly correspond to the brightness levels of the artefacts. But it so happens, at times, that some pixels of the artefacts have brightness values the same as that of soft tissue brightness in the ROI. Hence assuming that all the filled bins of the histogram to represent artefact intensity levels will lead to falsely identifying some tissue pixels as artefacts. In order to minimize the selection of these false positive pixels, we divide the gray level range [0,255] into three parts from 0-100, 101-200 and 200-255 respectively. The histogram peaks in each of the three parts is taken as the intensity level of the artefacts. The division of histogram into three levels is empirical and based purely on the best results obtained on multiple random trials performed by varying the intensity ranges.

3) Suppressing artefact intensities: Having estimated the artefact intensity levels, the next step is to suppress it from the ROI image $f_r(x, y)$, which allows it to be treated as an irregularly sampled image facilitating the use of a modified version of the Projection onto Convex Sets (POCS) algorithm to restore the image (discussed in section II-B).

Let the artefact intensity levels be represented by a threshold set $\mathcal{T}$ given by

$$\mathcal{T} = \{T_1, T_2, T_3\}. \tag{6}$$

We define the binary artefact mask $b_a(x, y)$ as

$$b_a(x,y) = \begin{cases} 1 & \text{if } f_r(x,y) \in \mathcal{T} \\ 0 & \text{otherwise} \end{cases} . \quad (7)$$

The binary artefact mask is further subjected to morphological operation of dilation with a 3×3 structuring element that includes the 8-Neighbours of the pixel under consideration. Dilation is done so that there will not be any step discontinuities when the image is restored.

The final ROI image, $g(x, y)$ with the artefacts removed is obtained by multiplying the ROI image $f_r(x, y)$ with $\bar{b}_a(x, y)$, the complement of the binary artefact mask

$$g(x,y) = f_r(x,y) \cdot \bar{b}_a(x,y). \quad (8)$$

Figure 4 shows the ROI image of Fig. 3, with the artefacts removed using the method described above. It can be seen that the machine induced artefacts are completely removed from the ROI. It is also observed that a few of the tissue pixels are also removed in the process, but all of these are restored to a fair degree of accuracy by the restoration scheme described in section II-B.

B. Stage 2: Image Restoration

A very well established technique to restore images is by the method of Convex Projections or more commonly known as Projection onto Convex Sets (POCS) method [13]. In order to restore the artefact removed pixels in our algorithm, we follow an approach similar to the one observed in [14], with a slight modification. Authors in [14] treat the restoration of the tampered images with watermarks as an irregular sampling problem and use POCS to iteratively restore the tampered parts of the image. As in [14], we use the basis vectors of the cosine transform for projection as it has been shown that it approximates a given signal better to give good reconstruction results.

We divide the input image $g(x, y)$ into blocks of size $B \times B$ pixels with a block overlap of $B/2$ pixels, $B > 0$, and apply Block Discrete Cosine Transform (BDCT) to obtain $G(u, v)$. The first projection operator P_1 is given by:

$$P_1 f = \begin{cases} F(u,v) & \text{if } u - v < a; 1 < a < B \\ 0 & \text{otherwise} \end{cases} \quad (9)$$

where $F(u, v)$ is the BDCT of $f(x, y)$. The significance of the projection in Eq. (9), is for the projection operator to act as a low pass filter to obtain a B band-limited image block.

Let $\triangle$ denote the set of all pixels that were removed during the artefact removal process. Then the second projecton operator P_2 is given by:

$$P_2 f = \begin{cases} f(x,y) & (x,y) \in \triangle \\ g(x,y) & (x,y) \notin \triangle \end{cases} . \quad (10)$$

The image is iteratively restored using the relation:

$$f^{(n+1)} = P_2 P_1 f^{(n)} \quad (11)$$

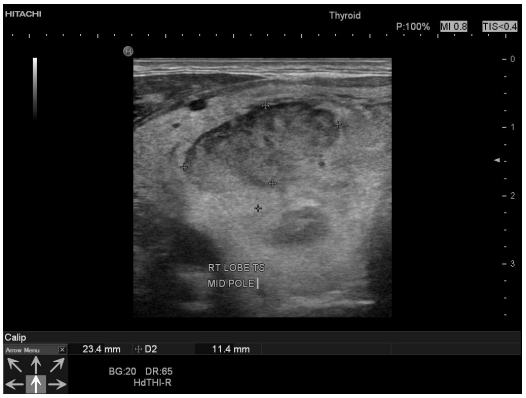

Fig. 3. Input 2D Ultrasound Image $f(x, y)$ of the thyroid gland having artefacts.

Fig. 4. ROI Image $f_r(x, y)$ with artefacts removed.

Fig. 5. Restored image $\tilde{f}$(x,y).

with

$$f^{(1)} = P_2 P_1 g. \quad (12)$$

Figure 5 shows the final output $\tilde{f}(x, y)$ after artefact removal and restoration using the proposed POCS method.

III. Results and Discussion

The proposed algorithm was implemented using Matlab 2008 and was executed on a dataset of 18 ultrasound images of the thyroid gland. Each image had at least one nodule with caliper marks and text material within the ROI. The images were acquired using Hitachi HI Vision Avius Ultrasound

Case Number	1	2	3	4	5
Average PSNR	39.78	40.48	38.94	39.62	39.67
Case Number	6	7	8	9	10
Average PSNR	39.02	40.33	40.11	41.06	40.91

TABLE I
RESTORATION QUALITY ANALYSIS

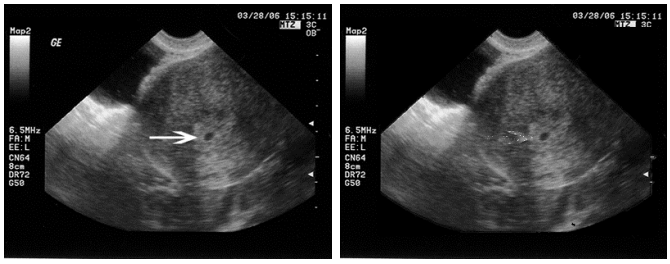

(a) Input (b) Output

Fig. 6. Restoration of a US image randomly downloaded from the internet

device and processed offline on an Intel(R) Core(TM) i5-2400 CPU @ 3.10GHz computer.

For the POCS algorithm, BDCT was performed on image blocks of size 64×64 pixels with a block overlap of 32 pixels and B=16. In order to qualitatively measure the performance of the proposed scheme, an additional 10 US images of the thyroid gland were acquired without any artefacts. Artefacts in the form of text material were introduced at random locations within the ROI of the image and was subjected to artefact removal and restoration. PSNR was calculated on the restored image to measure the quality of restoration. The simulation was carried out 50 times, with artefacts embedded at random locations in each simulation, on each image in the dataset. Table I shows the average PSNR value for all the images in the dataset. It can be seen that the images have PSNR values greater than 38dB indicating the high quality of restoration.

Apart from measuring the PSNR values, a subjective analysis was also performed; where the participant pool (n=17), that included clinicians and medical imaging researchers, was asked to give a rating on a scale of 1-5, indicating their opinion on the quality of restoration on the 18 images in the dataset. A score of 1 was given when a participant strongly agreed that all of the artefacts were removed and a score of 5 was given when a participant strongly disagreed that the artefacts were removed. The results showed that for 8 out of the 18 cases, the participants strongly agreed that the artefacts were completely removed in the restored image; the participants somewhat agreed that the artefacts were removed for 8 out of 18 cases, while the participants neither agreed nor disagreed on the artefact being removed for 2 of the 18 cases.

The algorithm was also run on a random ultrasound image downloaded from the internet to check the generality of the algorithm. Figure 6(a) shows an ultrasound image of a foetus with an arrow mark, given as input to the algorithm. Figure 6(b) shows the output of the algorithm where most of the artefact has been removed by the algorithm. The algorithm, in general, was able to fully suppress those artefacts that were present at locations having smooth transitions of tissue gray levels and restore the image without any trace of the artefacts. The artefacts that were present at the locations of sudden gray level discontinuities, like edges of cystic nodule walls etc., were suppressed fully in the first stage, but restoration process resulted in a smooth gray level profile, instead of a sharp edge, at the locations where the artefact was present . This is due to the first projection operator which acts as a low pass filter, essentially producing a blurring effect during the restoration process. In both of the above mentioned cases, the artefacts had an arbitrary but constant intensity value. The algorithm failed to suppress those artefacts that did not have a constant intensity level and hence these were still present even after the restoration process.

In conclusion, we have developed an algorithm that automatically detects manually induced artefacts in an ultrasound image and restores the image as accurately as possible with a high quality so long as the artefacts have a constant intensity level and are embedded at locations having a smooth gray level profile.

REFERENCES

[1] N. Archip, R. Rohling, P. Cooperberg, H. Tahmasebpour, and S. Warfield, "Spectral clustering algorithms for ultrasound image segmentation," *Medical Image Computing and Computer-Assisted Intervention–MICCAI 2005*, pp. 862–869, 2005.

[2] S. Armato, III et al., "The Lung Image Database Consortium, (LIDC) and Image Database Resource Initiative (IDRI): A Completed Reference Database of Lung Nodules on CT Scans," *Medical Physics*, vol. 38, no. 2, pp. 915–931, Feb 2011.

[3] A. Dunstan, C. Silkowski, and C. Odwin, *Emergency Medicine Sonography: Pocket Guide to Sonographic Anatomy and Pathology*. Jones & Bartlett Learning, 2010.

[4] Y. Fang and J. Wang, "Selection of the number of clusters via the bootstrap method," *Computational Statistics & Data Analysis*, vol. 56, no. 3, pp. 468–477, mar 2012.

[5] A. K. Jain, "Data clustering: 50 years beyond K-means," *Pattern Recognition Letters*, vol. 31, no. 8, SI, pp. 651–666, june 2010.

[6] T. Lange, V. Roth, M. Braun, and J. Buhmann, "Stability-based validation of clustering solutions," *Neural Computation*, vol. 16, no. 6, pp. 1299–1323, june 2004.

[7] B. Matheus and H. Schiabel, "Online Mammographic Images Database for Development and Comparison of CAD Schemes," *Journal Of Digital Imaging*, vol. 24, no. 3, pp. 500–506, Jun 2011.

[8] N. S. Narayan, P. Marziliano, and C. G. L. Hobbs, "Echogenicity based Unsupervised Segmentation of Ultrasound Images of the Thyroid Gland," *To be submitted to IEEE Trans. on Medical Imaging*, 2013.

[9] R. Nishikawa, M. Giger, K. Doi, C. Metz, F. Yin, C. Vyborny, and R. Schmidt, "Effect Of Case Selection On The Performance Of Computer-Aaided Detection Schemes," *Medical Physics*, vol. 21, no. 2, pp. 265–269, Feb 1994.

[10] syngo.via Mobile Applications, January 2013. [Online]. Available: http://healthcare.siemens.com/medical-imaging-it/syngoviaspecialtopics/syngoviamobileapplications

[11] Z. Volkovich, Z. Barzily, G.-W. Weber, D. Toledano-Kitai, and R. Avros, "Resampling approach for cluster model selection," *Machine Learning*, vol. 85, no. 1-2, SI, pp. 209–248, oct 2011.

[12] J. Wang, "Consistent selection of the number of clusters via crossvalidation," *Biometrika*, vol. 97, no. 4, pp. 893–904, dec 2010.

[13] D. Youla and H. Webb, "Image restoration by the method of convex projections: Part 1 - theory," *Medical Imaging, IEEE Transactions on*, vol. 1, no. 2, pp. 81 –94, Oct. 1982.

[14] X. Zhu, A. Ho, and P. Marziliano, "Image authentication and restoration using irregular sampling for traffic enforcement applications," in *First International Conference on Innovative Computing, Information and Control, ICICIC '06.*, vol. 3, Sept 2006, pp. 62 –65.